Received: 15 November 2022 | Revised: 21 February 2023 | Accepted: 30 March 2023

DOI: 10.1002/ese3.1457

ORIGINAL ARTICLE

Simultaneous working fluid and expander selection method for reaching low-threshold technology organic Rankine cycle (ORC) design

Axel Groniewsky[1] | **Réka Kustán**[1] | **Attila R. Imre**[1,2]

[1]Department of Energy Engineering, Faculty of Mechanical Engineering, Budapest University of Technology and Economics, Budapest, Hungary

[2]Department of Thermohydraulics, Centre for Energy Research, Budapest, Hungary

Correspondence
Axel Groniewsky, Department of Energy Engineering, Faculty of Mechanical Engineering, Budapest University of Technology and Economics, Műegyetem rkp. 3, H-1111 Budapest, Hungary.
Email: groniewsky@energia.bme.hu

Funding information
National Research, Development and Innovation Fund of Hungary, Grant/Award Numbers: 2020-3.1.1-ZFR-KVG-2020-00006, Sustainable Development and Technologies National, TKP2020 NC, BME-NC, ÚNKP-21-5; János Bolyai Research Scholarship of the Hungarian Academy of Sciences, Grant/Award Number: Bolyai

Abstract

Maximizing the utilization of an available source serves as the ideal approach, provided that only technical factors are considered. For sources with low heat flux, however, cost-effective solutions are more suitable due to the minimal net power generated, regardless of the effectiveness of the energy conversion. In such cases, utilizing low-threshold technology may be the most fitting solution, the layout of these cycles should be simple and inexpensive. In the case of organic Rankine cycles (ORCs)-based power cycles, this means the omission of superheaters or recuperative heat exchangers and the use of simple expanders and small heat exchangers. Simplifying the design, however, requires additional considerations about the elementary steps of the cycle. This work presents a procedure to select favorable working fluids for ORC while considering the expander's internal efficiency. The criteria for favourability is to have a nonideal expansion process starting and ending in (or very near) saturated vapor states to avoid problems related to wetness/dryness between the given maximal and minimal expansion temperatures. It is demonstrated that the design can be simplified under the simultaneous working fluid and expander selection method presented in this study, regardless of the type and isentropic efficiency of the expander. The resulting methodology applies the novel classification of working fluids using the sequences of their characteristic points on temperature-entropy space. The proposed approach is illustrated with a case study finding optimal working fluid for an ORC system fitted to industrial waste heat, a low-temperature geothermal, and a cryogenic heat source.

KEYWORDS
organic Rankine cycle (ORC), real expansion process, *T–s* diagram, working fluid selection

1 | INTRODUCTION

Organic Rankine cycles (ORC) transfer heat into shaft work or further to electricity if required. The cycle layout is similar to the one used by Rankine cycles (RC), but the operating conditions are different. ORC is applied under circumstances where it outperforms RC, typically for heat sources below 350°C (such as waste heat, geothermal heat, solar ponds, or biomass-based heat) and in the low power range (produced electricity only rarely exceeds the 20 MW_e[1]). Therefore, the construction of the units and the cycle's working fluid is also different. Because the most significant differences stem from the applied working fluids, many research papers address the issue of designing a new fluid[2] or selecting it from an already-known database.

The selection procedure is a multicriterion optimization problem whose criteria include, among many others, physical and thermodynamic properties, chemical stability and compatibility, safety (including toxicity and flammability), production costs, availability, previous experience with the material or with similar compounds, and environmental impacts.[2–4] Some of the properties comprise many parameters, such as thermodynamic properties require the investigation of liquid and vapor density,[5] latent heat of vaporization, liquid heat capacity,[6] viscosity,[7] thermal conductivity,[8] melting point temperature,[9] critical temperature, and pressure. In contrast, environmental impact is described only with ozone depletion potential (ODP) and global warming potential (GWP).[10,11]

The number of describing parameters shows that the thermodynamic optimum is perhaps the most complex problem to address.[12–14] Preferences may change the key factors slightly, yet fundamental properties influencing the outcomes are easily identifiable, regardless of the circumstances. Even though the optimum behavior of an ORC is not directly connected to the isentropic behavior of the fluids,[15] the shape of the saturated vapor line of the selected fluid in the *T*–*s* diagram plays an important role[16] when the purpose is to maximize the power output or when cycle efficiency is to be improved.[17,18] Namely directly affecting the layout and indirectly affecting the investment and operational costs.

As the shape of the saturated vapor line among the indicators that form the basis of the comprehensive analysis is heavily weighted in the evaluation,[19] the present work focuses on the fluid selection based on its saturated vapor line.

Although the focus on increasing energy efficiency puts the utilization of low-flux heat sources in the spotlight, only a limited amount of energy can be extracted from such sources. As the expected net power is small, the costs that can be considered reasonable and justified are limited. To ensure the profitability of such investments, an ORC unit providing only a few kW of power cannot cost more than a few thousand euros. Therefore, in many cases, a simplified ORC layout—containing a pump, a liquid heater/evaporator, a simple expander, and a small condenser with no superheater or recuperative heat exchanger or droplet-resistant expander—is more important than even a significant improvement in the thermal efficiency, if it would lead to a considerable increase in investment costs. This study introduces a simple method to find a working fluid (identified by name/chemical identifier) and a fitting expander (characterized by internal efficiency) which—if a suitable fluid database is available—guarantees a simplified layout under a given inlet–outlet expansion temperature pair. The selection procedure assists with thermodynamic solutions that may exploit low-flux heat sources, even at low technical content and investment costs.

2 | IMPORTANCE OF THE SHAPE OF THE SATURATED VAPOR LINE IN THE *T*–*S* DIAGRAM

Based on the established criteria of Tabor and Bronicki,[20] working fluids are either wet, isentropic, or dry types, depending on whether the final state of an isentropic expansion, starting from a saturated vapor phase, is in the two-phase region, saturated, or superheated vapor states, respectively.

As water is a wet fluid, the layout of a simple Rankine cycle is similar to an ORC using a wet working fluid (Figure 1A,B). After leaving the condenser in a saturated liquid state (1), the pump compresses the liquid (2). Then heat is transferred to the fluid through an economizer until reaching a saturated liquid state (3), an evaporator until reaching a saturated vapor state (4), and a superheater until reaching a superheated vapor state (5). The superheated vapor expands in the expander before reaching the condenser in a two-phase region (6). Higher moisture content in the exit of the expander increases the risk of droplet erosion which can be reduced by a superheater ($6^* \rightarrow 6$).

Nevertheless, if dry fluid is used (Figure 1C,D), the expansion terminates in the superheated vapor region (6), requiring no superheater. The drawback of this solution is the increasing heat load in the condenser, requiring a recuperative heat exchanger (6, 7) before condensation.

However, the ideal solution is to use isentropic fluids where—at least theoretically—a finite part of the

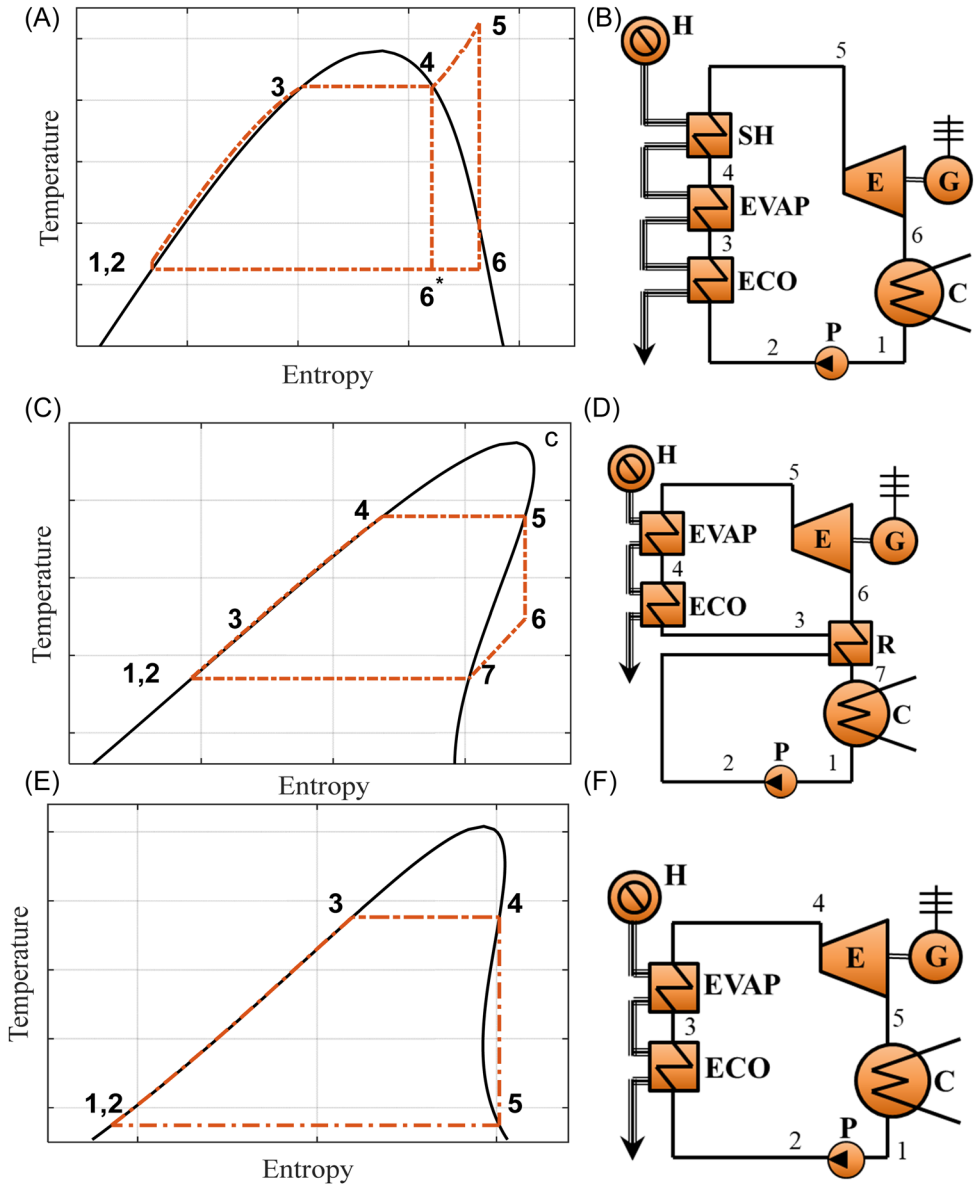

FIGURE 1 *T–s* diagrams and corresponding ORC layouts for wet (A, B), isentropic (C, D), and dry (E, F) working fluids. H, SH, EVAP, ECO, P, C, E, R, and G stand for heat source, superheater, evaporator, liquid heater (economizer), pump, condenser, expander, recuperative heat exchanger, and generator, respectively.

saturated vapor branch is a straight line with an infinite slope. In this case, expansion starts (4) and terminates (5) in a saturated vapor state, requiring neither superheater nor recuperator, enabling a cost-effective and reliable operation. A similar process can be achieved in the given temperature range with the so-called real isentropic fluids (Figure 1E,F) having inverse S-shaped saturated vapor lines.[21,22]

In the following, a method is presented that recommends working fluids from a publicly available, high-accuracy working fluid database, taken from the NIST Chemistry WebBook[23] and RefProp 9.1,[24] for a given heat source and heat sink temperature pairs at which the expansion starts and terminates in a saturated vapor state. Although there are numerous other potential working fluids and other—mostly commercial—databases, the NIST-based ones were preferred due to the undoubted accuracy of the reported data.

Most fluids in the database are traditionally classified as dry or wet.[25] At the same time, only a significantly smaller proportion has the inverse S-shaped saturated vapor branch, where all kinds of expansion processes (reaching wet or dry region or saturation state) can be realized, depending on the initial point and the length of the expansion. However, in this work, for more precise classification, subclasses are used, introduced by Györke

et al.[21] when establishing novel classifications. These subclasses are distinguished by their characteristic points on the saturated curve: A is the initial point of the saturated liquid curve, C denotes the critical point, M indicates the local entropy maxima, N represents the local entropy minima, while Z is the closing point of the curve. According to this classification, the diagrams in Figure 1. may be classified as ACZ (Figure 1A), AZCM (Figure 1C), or ANCMZ (Figure 1E) types.

3 | SELECTION OF WORKING FLUIDS FOR ISENTROPIC EXPANSION

As has been already mentioned, isentropic working fluids—in the sense of having an infinite slope in a finite part of the vapor branch of the *T*–*s* diagram—do not exist, yet isentropic processes from saturated vapor to another saturated vapor state can be realized in some working fluids. An illustrative example is given for the case of 2,2-dichloro-1,1,1-trifluoro-Ethane, often referred to as Freon-123 or R-123 and identified in chemical databases as CAS 306-83-2. This case can be seen in Figure 2A, where isentropic expansion occurs between points 1 and 2; the expansion proceeds through dry states, therefore, problems related to droplet formation are eliminated. Since the expansion terminates in a saturated vapor state (point 2), condensation can be started immediately. In this way, problems related to residual heat (like for state 6 in Figure 1C)—efficiency loss, excess heat load for condenser—are also eliminated. This expansion process can be labeled as "from saturated vapor state to another saturated vapor state through dry states" type one.

Since not all fluids included in the database have a refrigerant (R) number (e.g., toluene), it is not possible to provide a consistent identification applying this nomenclature. Instead, the well-established and routinely used CAS Registry Number identifier was used. A table presenting the common names, the CAS numbers, and the R-numbers (where available) is to be found in Appendix A.

The diagram shown in Figure 2. a is a so-called ACNMZ-type, where these letters correspond to the five characteristic points of the curve ranked by their entropy values.[13] It is important to mention that from point 1, only point 2 can be reached this way. Therefore, having an inlet-outlet expansion temperature diagram, one point (given by a temperature pair) represents this scenario (Figure 2B, point (1;2)). This is not the only route; moving from 3 to 4 or 5 to 6 through isentropic steps is also possible. By plotting all points representing these isentropic expansion processes, a material-specific curve is obtained in the maximal–minimal expansion temperature diagram.[22,26,27] For R-123 (the material described by the *T*–*s* diagram of Figure 2A) this curve is shown in

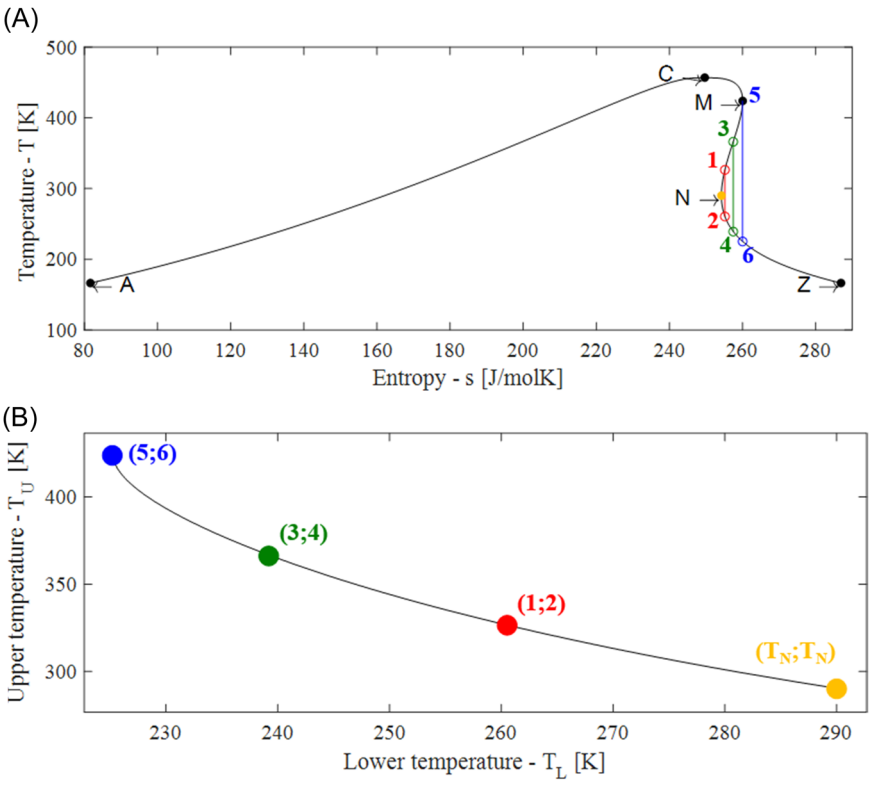

FIGURE 2 (A) *T*–*s* diagrams of Freon-123, marking four various ideal expansion routes and the diagram showing the potential maximal–minimal pairs of "from saturated vapor state to another saturated vapor state through dry states" expansion processes (B). Corresponding expansion routes are marked by the same colors. Here—as well as later—the bracketed expansion processes (e.g., (1;2) are marked as initial-final states instead of corresponding temperature values).

Figure 2B. The lower endpoint of the curve represents the shortest expansion possible, with the initial state at $T_N + \delta$ and the final state at $T_N - \delta$, where T_N is the temperature for point N and δ is an infinitesimally small temperature difference, approaching zero. It is similar to where the inlet and outlet expander temperatures—or maximal and minimal cycle temperatures when an ideal cycle is investigated—are identical. Thus, there will be neither temperature difference nor utilizable energy.

Regarding the structure and design of the maximal-minimal temperature diagram, a more detailed explanation is given in Section 5. This characteristic expansion curve can be prepared for all materials showing a reverse S-shaped saturated vapor branch on the *T*–*s* diagram. Using the NIST Webbook,[23] this has been done for nearly 30 pure compounds. The result[22] can be seen in Figure 3.

These curves can be referred to as isentropic expansion route curves, constructed from individual points, representing isentropic expansion processes from saturated vapor to another saturated vapor state. The straight orange line connecting the endpoints (NN) represents the case where the maximal and minimal expansion temperatures are identical. Below this line, the minimum temperature would be above the maximal one; therefore, this region would represent physically impossible processes. The working fluids are marked by their CAS number and colored according to their classes.[21]

A heat source-heat sink pair with well-defined temperatures can give a fair estimate for the maximal and minimal expansion temperatures. Therefore, any given heat source–heat sink pair can be represented by a point on the inlet–outlet expansion diagram (Figure 3). Two minimal–maximal temperature pairs are marked, one for (213 and 293 K), labeled as CA (related to cryogenic cold side and environmental air "hot" side) and one for (300 and 472 K), labeled as AW (related to cold air cold side and medium waste heat hot side), marking situations for two different heat recovery scenarios. In the first case, a cryogenic liquid—for example, LNG—can be used as heat sink and the environment as the heat source.[28,29] The heat source could be a flue gas in the second case, while the heat sink is the environment.[30,31]

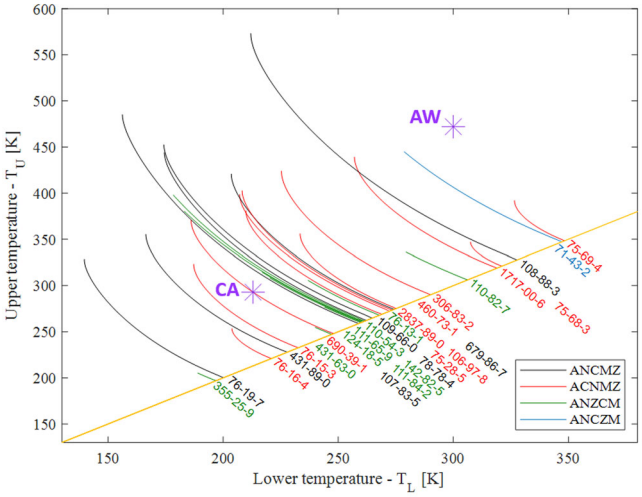

FIGURE 3 The curves represent potential "from saturated vapor state to another saturated vapor state through dry states" expansion processes for 29 working fluids. Materials are identified by their CAS numbers. Colors mark classes of working fluids. Two heat sink—heat source scenarios are marked (see text).

For the cryogenic process (cryogenic heat recovery, also called cold energy recovery, where the heat sink is a low-temperature, cryogenic fluid), working fluids are easily found with the exact—or nearly exact—saturated vapor to saturated vapor isentropic expansions. This is true not only for the marked CW case; as the densely spaced curves show in this temperature field (Figure 3), heat sink temperatures should be chosen in the cryogenic range. In the CW case, the optimal working fluid for a simple configuration design would be 1,1,1,3,3, 3-Hexafluoropropane (R236fa, CAS 690-39-1). At slightly higher heat sink temperatures, lines are more numerous; therefore, more than one suitable working fluid candidate is available in that cases.

Concerning the other waste heat recovery scenario AW (where cold air can be used as a heat sink), the nearest curves are very far; therefore, this method cannot find an adequate candidate, even though existing nominees have not been preselected for other criteria. Increasing the number of potential working fluids could help. Unfortunately, very accurate, well-established *T*–*s* data do not exist with a high amount of pure fluids; commercial software for ORC design often uses simplified models with low-accuracy equation of states to estimate entropy, and they might yield erroneous data. Therefore this research relies on a highly accurate NIST database, where the number of fluids is limited. There are two other ways to solve the expansion of the temperature range covered by the expansion route curves, which will be explained in the following passages.

4 | PARTIAL EXPANSION IN THE WET REGION

If, during expansion, the working fluid enters the wet region, the risk of droplet formation and erosion increases, as well as the mechanical loss due to the breaking effect on the rotor caused by the liquid impingements. At the same time, the expansion,

terminated to the superheated region, also limits the range of applicability of the working fluid and the maximum power output. The figures show two cycles (hatched in the figure). The expansion starts and terminates in saturated vapor states in both cases, yet the difference between the two expansions is significant. While the isentropic expansion in the first case (gray-hatched) goes through the saturated and the superheated vapor region only (1, 2, 3, 4, 5), in the second case (red-hatched), it proceeds the other with expansion through the wet region (1, 2, 3*, 4*, 5).

In Figure 4, three different isentropic expansion routes are identifiable; they all start and terminate in saturated vapor states (4*, 4, 5). The first one is the "wet region only" expansion process (4*, 4) because it proceeds through wet states. It resembles in some sense to the ones seen in wet fluids except for terminating in the saturated vapor state instead of the wet region. Also, in a traditional wet expansion (in a wet working fluid), the liquid ratio increases continuously as the expansion proceeds in the mixed-phase, while in this case, the initial increase will be followed by a decrease, and at the end of the expansion, the working fluid will be in a saturated vapor state once again. However, this expansion process, being the second and third types better, is not considered for real isentropic fluids in this study.

The second is the superheated vapor region expansion process (4, 5) discussed in the previous passage; they are the preferred expansion scenario for ORC technology.

Finally, the third one, the partially wet, partially superheated expansion process (4*, 5), which requires some further scrutiny. Only the initial part of the fast expansion process takes place in the wet region. Due to the fastness of the process—which is general for adiabatic expansions—the time for the fluid spent in the wet region is very limited. Droplets might be formed in this region, causing some wetness-related problems, but the wetness forms and disappears very quickly; therefore, the caused problems might be negligible. Additionally, it could be assumed that the working fluid remains in a metastable vapor state,[32,33] avoiding droplet formation. This is analogous to the process seen in the Wilson-zone of steam Rankine cycle. For water (and similarly, for other materials, too), the superheated vapor does not necessarily have time to condense when entering the two-phase region during expansion. The process terminates without creating a liquid phase and discharging latent heat of evaporation. Nevertheless, the temperature of the subcooled vapor drops below the saturation temperature. The probability of subcooling depends on the velocity of expansion of the vapor: $\dot{p} = -1/p \cdot \partial p/\partial \tau$, where τ is time.[34]

It should be emphasized that the subcooled vapor state is metastable in the Wilson region and disappears when thermodynamic equilibrium is reached.

When the expansion starts from or near the saturated vapor state, the medium does not have time to accelerate and enters the metastable zone as a wet fluid. Regardless, there will be no erosion in the rotor if the fluid reaches the saturated vapor phase before leaving the inlet valve. The outcome depends on the type of expander, the working fluid, and the operating conditions, especially from the relative position of the initial state between the critical point and local entropy maxima and the average value of $\dot{p}$. The notion of enlarging the media's scope in this manner may seem counterintuitive. However, energy conversion systems such as the organic flash cycle (OFC) are based on two-phase expansion.[35] Thus, the possibility of partial wet expansion in the inlet will also be considered in the following parts.

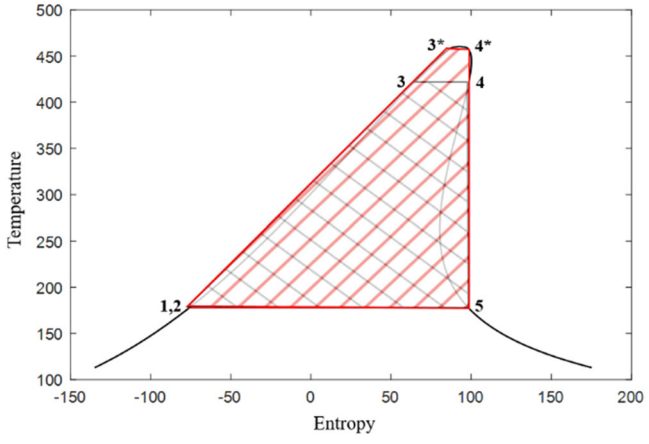

FIGURE 4 Comparison of the schematic *T*–*s* diagram of two reversible cycles, one with the expansion in the superheated vapor region only (1, 2, 3, 4, 5), the other with the expansion in a partially wet, partially superheated region (1, 2, 3*, 4*, 5).

5 | DESIGN OF T_L–T_U DIAGRAMS FOR EXTENDED ISENTROPIC EXPANSION PROCESSES IN THE TWO-PHASE REGION

Based on the novel classification,[21] pure working fluids are categorized by the entropy sequences of their primary and secondary characteristic points on their saturation line in the *T*–*s* diagram:

(1) Points A and Z: initial and final points on the saturation line with the triple point temperature.
(2) Point C: critical point with the highest temperature value, separating the saturated liquid (A–C) and vapor lines (C–Z).

(3) Points M and N: local or global entropy extrema.

As primary characteristic points, A, Z, and C can be found in all pure fluids. Among the secondary ones, M is found for dry and isentropic, while N is only for isentropic ones.

Among the eight possible sequences, ACZ represents wet, ACZM, and AZCM dry, while ANZCM, ANCZM, ANCMZ, ACNMZ, and ACNZM represent "real" isentropic fluids. Real refers to the fact that these classes have reverse S-shaped saturated vapor lines; therefore, it is possible to have an isentropic "saturated vapor state to another saturated vapor state" transition with them, described in Section 3. Neither ACZM nor ACNZM fluids have been found so far.[21,36] Subjects of the current investigation are the "real" isentropic fluids when expansion is assumed to be reversible and adiabatic, but in later passages, wet fluids under real expansion conditions will also be studied.

The T–s diagram of a traditional ACMNZ working fluid (Freon 123, already investigated in Section 3) is shown in Figure 5. It is possible to construct isentropic expansion processes initiated and terminated on the saturation vapor line; two of them are marked by straight lines. The blue one (4, 5) starts from the local entropy maxima (point M) and proceeds throughout the superheated vapor region (solid line), while the red one (1, 3) enters the two-phase region in the high-pressure section of the expansion (dashed line) and goes through the superheated vapor region before reaching the saturated vapor state (solid line). Each expansion can be clearly described by the temperature at which the process starts (T_U) and the temperature at which it ends (T_L). Suppose all possible expansion processes of working fluid are plotted with temperature point pairs; a single curve will represent the given material—the extended version of the curves shown in Figure 2—on an upper and lower temperature diagram (Figure 5B).

All ideal expansion routes of freon 123, initiating above and terminating below the N point, on the saturated vapor line, are shown in Figure 5B. The blue marker represents a superheated vapor region expansion process (from 423 to 225 K), with the highest upper temperature possible, separating partly or entirely wet expansions (dashed line) from superheated vapor region expansion processes (solid line). The red marker with solid fill (2, 3) represents an expansion taking place in the superheated vapor region from 353 to 245 K. Finally, the red marker without fill (1, 3) denotes an expansion in the partially wet, partially superheated region; dashed line represents all similar point pairs. Expansions in the wet region only (1, 2) have high T_U and T_L temperatures and are located on the upper right side of the dashed line outside the section ($T_L = 353$ K; $T_U = 453$ K) shown in the T_L–T_U field; being unfavorable ones, they are not shown here.

The four different T–s diagrams of the four different isentropic subclass working fluids are shown in Figure 6 with four representative samples: ACNMZ—freon 123

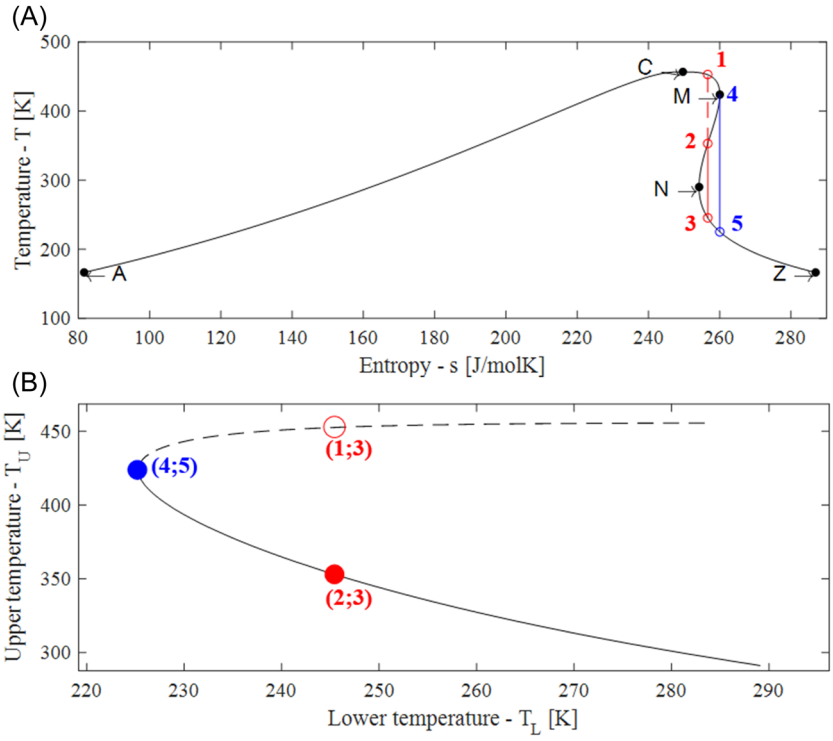

FIGURE 5 Isentropic expansion processes for freon 123 (306-83-2). (A) Extended adiabatic and reversible expansion processes in the two-phase region (B) Possible expansions with given starting (upper) and ending (lower) temperature; dashed part where the initial points of the processes are in the C–M section of the saturated vapor curve, while the solid ones represent the expansions started in the M–N section. Points (2;3), (4;5), and (1;3) represent the expansion processes from 353 to 245 K; 423 to 225 K, and 453 to 245 K, respectively.

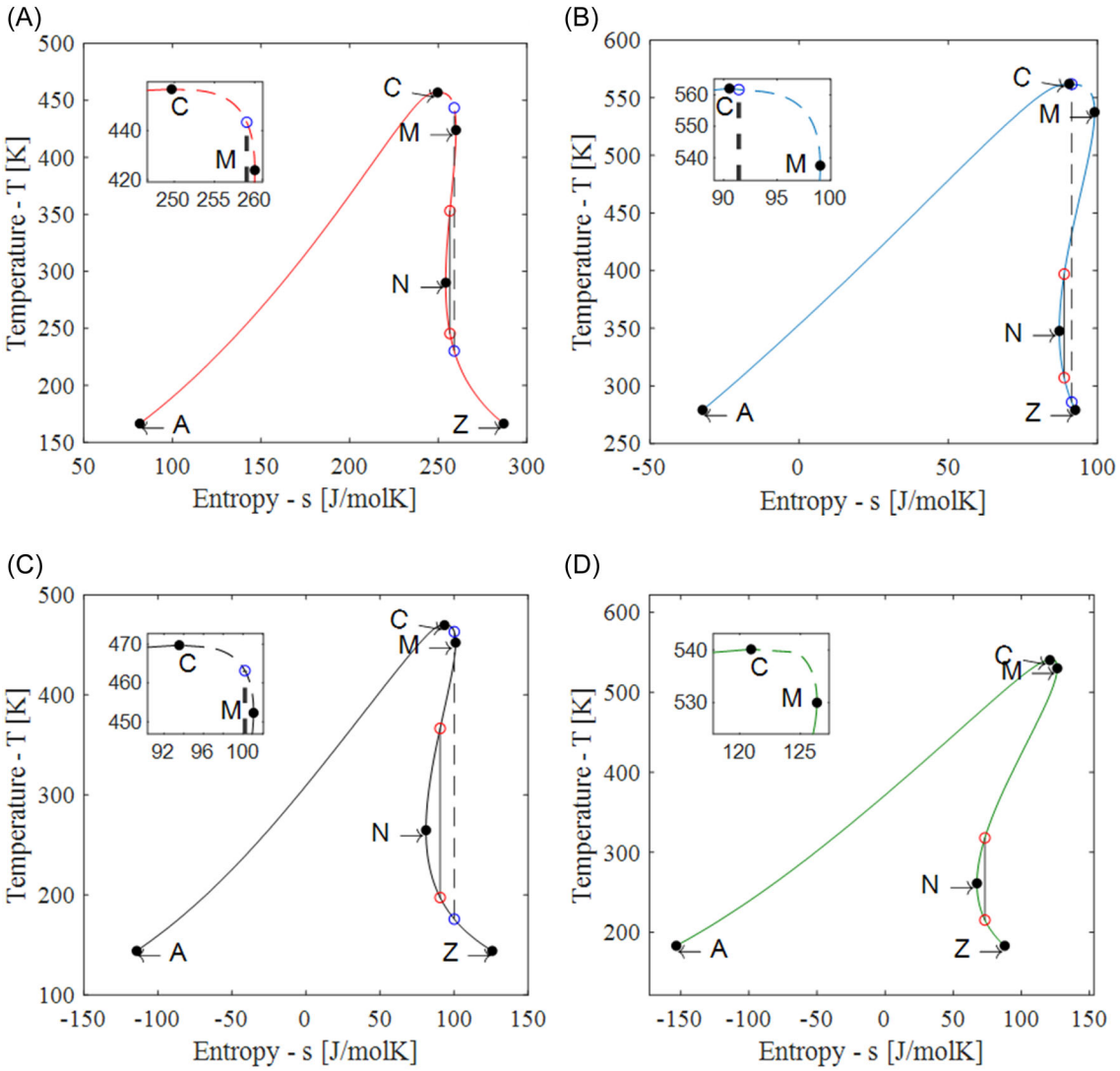

FIGURE 6 Four potential isentropic expansion routes for working fluids classified as ACNMZ (A: freon 123, CAS 306-83-2), ANCZM (B: benzene, CAS 71-43-2), ANCMZ (C: Pentane, CAS 109-66-0), ANZCM (D: heptane, CAS 142-82-5). Dashed lines mark expansion routes starting in C–M, and expansion routes starting in M–N are marked by solid lines.

(A), ANCZM—benzene (B), ANCMZ—pentane (C), ANZCM—heptane (D). The extent to which the applicability of a working fluid is raised when expansion in the wet region is considered depends on how far apart the temperatures of points C and M are. For freon 123 and benzene, the distance is significant enough to be worth considering, but not in the case of pentane or heptane. Also, for pentane and heptane, the M point is close to the critical point; therefore, an expansion initiated from the C–M part of the saturation curve could cause anomalies due to the proximity of the critical point.[37] Since the entropy of Z is just slightly above the value of C, only the immediate vicinity of point C could be considered as the starting point for the expansion; therefore, similar problems related to critical anomalies would emerge for benzene.

Figure 6 shows two ideal (isentropic) expansion routes on three of the four *T*–*s* diagrams. The ones starting in M–N section are marked with solid lines and red initial and final points, and the ones related to the C–M section have dashed lines and blue initial and final points. It has to be noted that ANZCM fluids have only adiabatic and reversible expansion routes initiating from the C–M section, which run entirely in the wet region due to their relative position to the other characteristic points. Thus, the applicability of the ANZCM fluids is not influenced by the C–M section. Nonetheless, it is beneficial to take the whole C–Z section into account when concerning the examination of the expansion routes.

T_L–T_U curves are not always continuous; there could be some discontinuity between parts representing

partially wet (1,3 in Figure 5B) and entirely superheated (2,3 or 4,5 in Figure 5B) expansions. Whether there is a gap in the curve depends mainly on the relative positions of the primary and secondary characteristic points, that is, the subclasses these materials belong to. Figure 7 shows a reduced T_L–T_U diagram with the example fluids taken from the previous example. Reduced scales are routinely used when properties or behavior of chemically different materials are to be presented on the same scale. Each curve shows one material, identified by its chemical identifier (CAS number), and just like earlier, a point on a curve describes one expansion process with a given starting (upper) and ending (lower) temperature. The dashed parts of the curves are expansion processes with initial points in the C–M section of the saturated vapor curve, while the solid part represents the expansions started in the M–N section.

Freon 123, as an ACNMZ type fluid, is a fine example of a continuous line (red line), just like ANCMZ pentane (black line). Isentropic expansion from the C–M section is not limited to ANCMZ fluids, but for the ACNMZ subclass, expansions cannot be initiated from a point lower than the entropy at characteristic point N. As Z has lower entropy than M, ANCZM fluids show gaps, as demonstrated by benzene (blue line). Since Z has lower entropy than C, ANZCM fluids, like heptane (green line), cannot initiate an isentropic expansion from the C–Z section, terminating in a saturated vapor state.

One can construct an expansion diagram for all materials available in the NIST database[23,38] similar to the one shown in Figure 3, extending the methodology's usability by including expansions starting on the part of the saturated vapor line located between points M and C. The minimal–maximal temperature pairs representing expansions through the superheated (dry) region are located below, while the wet-dry mixed expansions are located above the T_U minima of the curves in Figure 8.

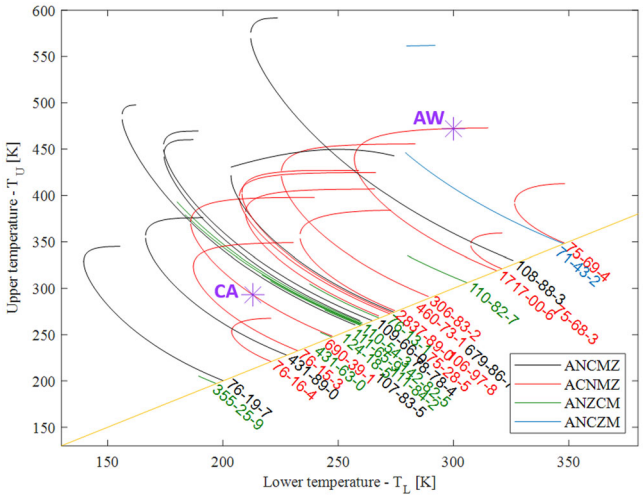

FIGURE 8 The curves represent potential "from saturated vapor state to another saturated vapor state through dry states" expansion processes for 28 working fluids (similar to Figure 3), including initially wet expansion processes. Materials are identified by their CAS numbers. Colors mark classes of working fluids. The two heat sink—heat source scenarios—for cryogenic case (213 K;293 K), labeled as CA, and for waste heat case (300 K; 472 K), labeled as AW—are marked. In both cases, perfectly matching working fluid can be found.

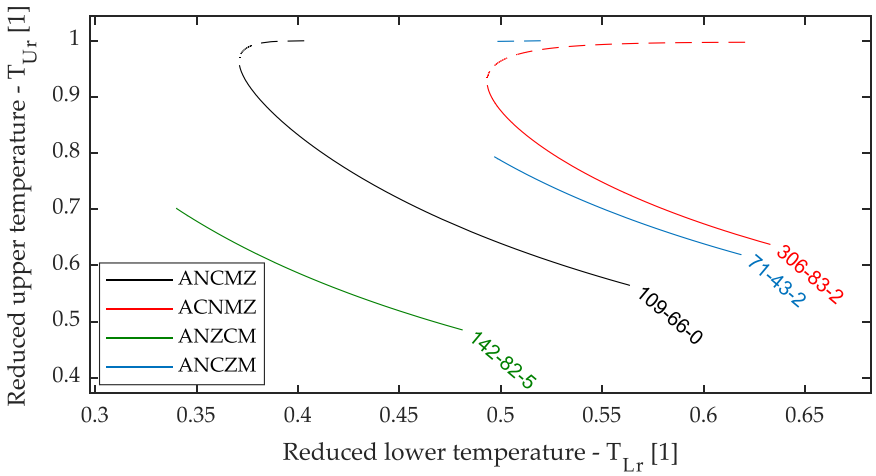

FIGURE 7 Potential expansion routes on reduced T_L–T_U diagram for four working fluids, identified by their CAS number. 306-83-2: freon 123, 71-43-2: benzene, 109-66-0: pentane, 142-82-5: heptane. Each curve shows one material, identified by its chemical identifier (CAS number), and a point on a curve describes one expansion process with a given starting (upper) and ending (lower) temperature. The dashed parts of the curves are expansion processes with initial points in the C–M section of the saturated vapor line, while the solid part represents the expansions started in the M–N section.

With the extended methodology, a suitable working fluid may be found for the waste heat recovery scenario, labeled AW and described in Section 3, without extending the databases. Namely, the extended temperature sets include the R140b (CAS 1717-00-6, 1,1-Dichloro-1-fluoroethane) running in the vicinity of point AW, representing a—from a thermodynamic point of view—potentially favorable solution.

6 | DESIGN OF T_L–T_U DIAGRAMS FOR IRREVERSIBLE EXPANSION PROCESSES

Even though this extension provides a broader temperature range covered by potential expansion routes, high-temperature cases are still underrepresented. Additionally, all the cases investigated so far were ideal (i.e., all expansions were isentropic). Real expanders have internal efficiencies (below 100%), showing deviation from ideal expansions. Among the turbines utilized for low-temperature heat recovery, only axial turbines operating in the MW_e power range exceeds the internal efficiency of 90%. Conversely, other turbine types operating in the kW_e range demonstrate significantly lower isentropic efficiencies. Table 1 presents the isentropic efficiencies of different expanders in the kW_e range, based on experimental results. Three expansions shown on the *T*–*s* diagram of Isopentane (2-methyl-Butane, CAS 78-78-4, a typical ANCMZ-type working fluid) are in Figure 9A. It can be seen that expansions with lower internal efficiencies are terminating at higher entropies than expansions with higher internal efficiencies. This deviation gives a new opportunity to find matching minimal–maximal temperature pairs with expander efficiencies below 100%. In this case, even wet working fluids might be suitable candidates for "saturated vapor to saturated vapor" type expansions, going through a region with relatively low wetness.[27,40]

Novel expansion route maps can be drawn for the working fluids (shown in Figure 9) with any given external efficiency value. Figure 9B shows the new curves representing 100%, 80%, and 60% internal efficiencies. All points between the 100% and 60% curves represent a case where an exact "saturated vapor state to another saturated vapor state expansion" can be found for a given working fluid (isopentane) with a given internal expander efficiency. Therefore, with this method, the cases will be more realistic (real expansion processes with less than 100% internal efficiency), and the temperature range covered by the curves will be broader. Thus, internal efficiency as a new variable allows for a more accurate working fluid selection for various heat sink–heat source pairs.

Allowing nonideal expansion routes and accepting that even though the expansion starts and terminates in saturated vapor states, it will proceed through a moderately wet region,[27,40] like the ones represented by the dashed lines in Figure 7, some of the wet (ACZ-type) working fluids can be included in the selection pool. For these materials, ideal (100% internal expander efficiency) expansion processes cannot be constructed between two saturated states, but it is possible to do that with nonideal expansion processes. Examples of dichlorodifluoromethane (CAS 75-71-8, R12) are shown in Figure 10. a, with two different internal efficiencies (80% and 60%), both well below 100%. The temperature pairs for a given internal efficiency value are also forming curves; they are

TABLE 1 Efficiency and power range of different types of ORC expanders.[39]

Radial turbines			Scroll expander			Screw expander		
Working fluid	**Output power (kW_e)**	**Efficiency (%)**	**Working fluid**	**Output power (kW_e)**	**Efficiency (%)**	**Working fluid**	**Output power (kW_e)**	**Efficiency (%)**
R123	6.07	58.53	R123	0.75	38	R218	20	60
R123	8.33	48–63	R123	1.54	86	R123	6.58	42.53
R123	534	84.3	R123	2.78	85,17	R123	8.35	73
R143a	400	82	R134a	0.557	78	R123	10.38	73.25
R134a	641.2	79.9	R245fa	-	84,9	R123	100–300	60–88
R245fa	~35	~65	R245fa	1.016	77,74	R134a	193.75	70.82
R245fa	177.4	68.1	R245fa	1.8	75,7	R245fa	-	~79
R245fa	250	63.7	R245fa	2.3	73	R245fa	~7	~60
R245fa	~1000	~85				R245fa	~8.5	60

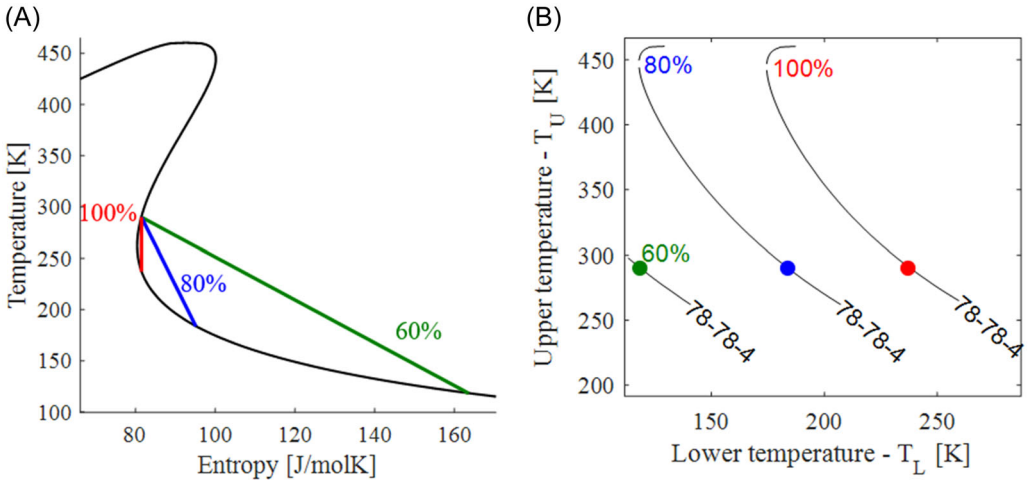

FIGURE 9 (A) The relevant part of the *T*–*s* diagram of 2-methyl-Butane (CAS 78-78-4), a typical ANCMZ-type working fluid, showing an ideal (red, 100% expander internal efficiency) and two real (80% [blue] and 60% [green] expander internal efficiencies, respectively), starting from the same initial saturated vapor state but terminating in different saturated vapor states. (B) The potential expansion routes of the same material with these three different internal efficiencies. Colored dots mark the expansion processes shown in part A.

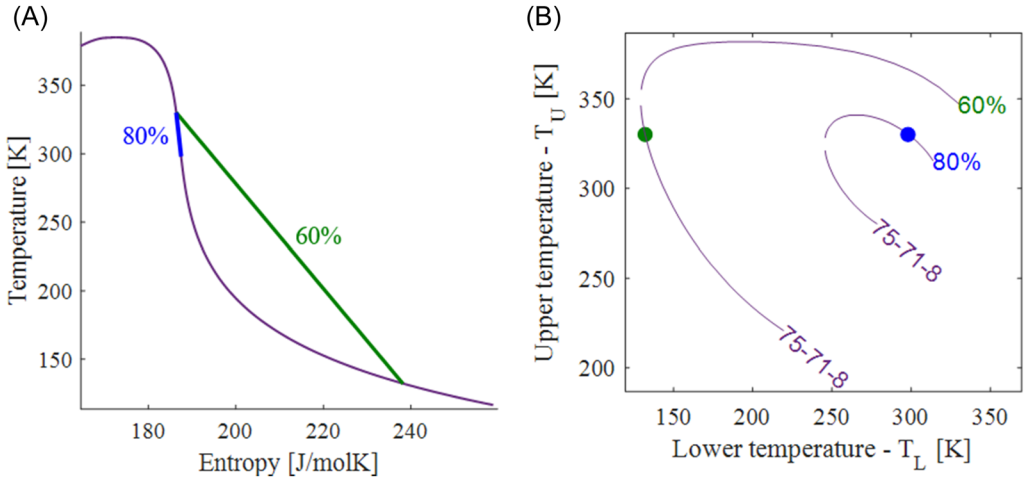

FIGURE 10 (A) The relevant part of the *T*–*s* diagram of Dichlorodifluoromethane (CAS 75-71-8, R12) is an ACZ-type nearly isentropic working fluid, showing two real expansion processes (80% [blue] and 60% [green] expander internal efficiencies, respectively), starting from the same initial saturated vapor state but terminating in different saturated vapor states. (B) The potential expansion routes of the same material at different temperatures with these two internal efficiencies. Colored dots mark the expansion processes shown in part A.

shown (for this working fluid) in Figure 10B. With the inclusion of wet working fluids, the pool of potential working fluids increased from 28 (real isentropic ones) to 69 (real isentropic and wet ones), concerning only the ones having high-accuracy temperature-entropy data obtained from the NIST database.[38]

The T_L–T_U diagram of irreversible expansion routes is assembled similarly to the reversible one, with consideration of the internal efficiencies of the expander units. Figure 11 shows the expansion processes from saturated vapor to saturated vapor states between 100% and 55% internal efficiencies with a 15% decline (shown in % in the bottom left corner). To construct the T_L–T_U diagrams, the properties of 69 materials were taken from the NIST database.[27] The color codes for each subclasses are identical to those used in the previous figures.

Figure 11A shows theoretically possible, adiabatic, and reversible (100%) expansion routes for multiple working fluids as a benchmark (identical to Figure 8). It is prominent that only real isentropic fluids are on the diagram. Subclass ACNMZ and ANCMZ materials are predominant, while ANCZM is represented by one fluid only, corresponding to the proportion of the isentropic subclasses in the database (10% ANCMZ, 16% ACNMZ, 13% ANZCM, 2% ANCZM, and 59% ACZ). In Figure 11B, presenting 85% isentropic efficiency expansions, wet

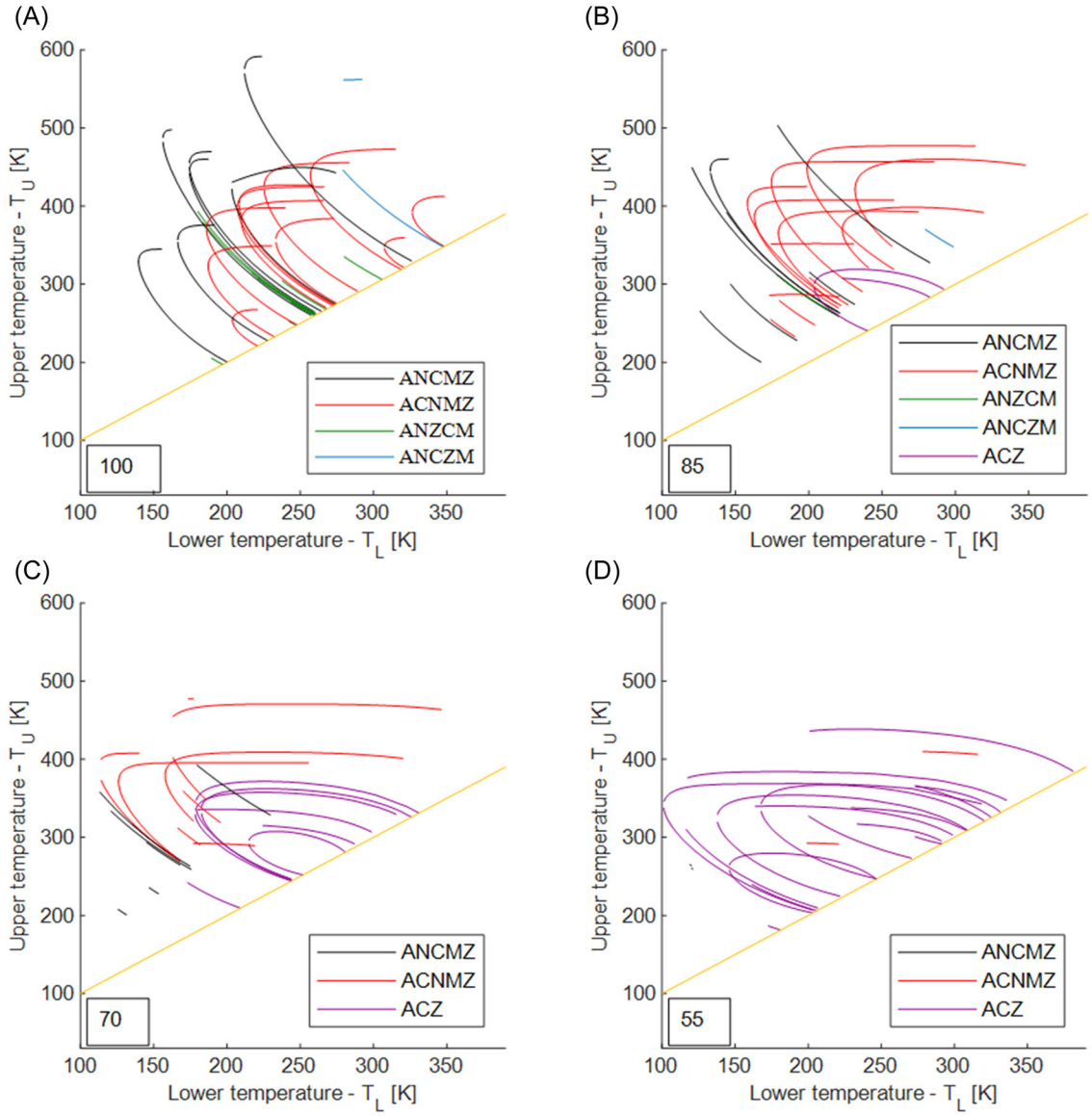

FIGURE 11 Potential expansion routes of different working fluid classes initiating and terminating in saturated vapor states under varying internal efficiencies; (A) adiabatic and reversible expansions; (B) expansions with 85% internal efficiency; (C) expansions with 70% internal efficiency; (D) expansions with 55% internal efficiency.

fluids (ACZ) appear in small quantities, while the number of ANZCM fluids drops significantly. For the 70% efficiency in Figure 11C, only three classes (ANCMZ, ACNMZ, and ACZ) remain, among which the solutions offered by ACNMZ are mostly expansion routes in the partially wet, partially superheated region. Wet fluids dominate the lowest 55% efficiency map in Figure 11D; other class offers no real alternative.

As a general rule, it can be stated that with decreasing isentropic efficiency, isentropic fluids detach from the enveloping curve (orange line) and become shorter while the presence of ACZ substances increases and become dominant in the T_U–T_L field. This conclusion is consistent with the proposal of Shahrooz et al.,[40] who suggested that ACZ fluids should not be eliminated from the candidate list just due to their types. When alternative expanders with lower isentropic efficiency are applied, it can reduce the superheat load on the evaporator without terminating the expansion process in the wet region, yet it also decreases the shaft work.

One can visualize that by marking a case with a given T_U–T_L pair and scrolling from 100% down to 50%, occasionally, some lines could intercept or give a near hit for the given point. Each hit marks a matching (working fluid; expander) pair for the case. At the end of the scroll, it is possible to use the set of these hits as a basis for further evaluation (environmental effect, production costs, availability, etc.), or if preselection has occurred

and the database only includes materials that meet all other required criteria, then the resulting fluids will be appropriate for practical use.

Based on the method, a Working Fluid Selector algorithm has been constructed to select the suitable working fluid for a given heat source and sink—characterized by their temperatures—from the point of view of (or simultaneously with) the expansion process. Figures 8, 9B, 10B, and 11 were produced with this program, and the results shown in the following case studies are obtained using it. Detailed information about the program can be seen in Appendix B and a video showing a real selection process can be found in the Supporting Information Materials.

In the following passage, three cases are investigated with realistic expander input–output temperature pairs to show the potential of this novel selection method.

7 | CASE STUDIES

ORC is always installed based on three fundamental information: heat source temperature (T_{source}), heat sink temperature ($T_{environment}$), and quantity of the available heat. However, when working fluid is selected for a tailor-made real cycle, heat transfer and expansion losses must be considered. Figure 12 compares an ideal (1, 2, 3, 4; blue) and a real (1*, 2*, 3*, 4*; red) ORC cycle using a schematic *T*–*s* diagram of an ANCMZ-type working fluid. Yellow and green lines represent the temperature profile of the heat source and heat sink, respectively.

Losses influencing the temperature range of operation for real cycles are the following: irreversibility in the pump (1*, 2*), and the expander (3*, 4*), pressure drop in the evaporator (2*, 3*) and condenser (4*, 1*), the need of subcooling the saturated liquid (1*) before the low-pressure side of the pump impeller to prevent onset cavitation.

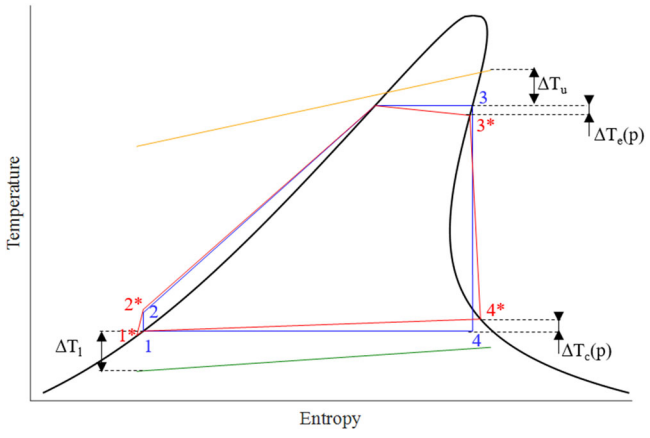

FIGURE 12 Comparison of real and ideal ORC cycles for given conditions.

Therefore, the upper-temperature limit (T_U) for the expansion, might be calculated as:

$$T_U = T_{source} - \Delta T_u - \Delta T_e(p), \quad (1)$$

where ΔT_u represents the temperature difference between heat source inlet and evaporation, while $\Delta T_e(p)$ is the temperature change due to pressure drop caused by flow resistance; both are characteristic values for the heat exchanger.

The lower temperature limit is determined similarly, using the temperature difference between heat sink inlet and condenser (lower ΔT_l) and the pressure-dependent temperature change of the condenser $\Delta T_c(p)$:

$$T_L = T_{source} + \Delta T_l + \Delta T_c(p), \quad (2)$$

This (T_U, T_L) temperature pair is to be used in Figure 11 as a characteristic point to select the most suitable working fluid after the isentropic efficiency of the expander is estimated based on vendor data (catalog), type, size, and other working conditions. As working fluids influence internal efficiencies, the estimation might require iteration.

The following examples are not real cases but only approximate models illustrating a favorable working fluid and expander selection procedure. Different heat sources and heat sinks are represented with different, realistic temperature limits, while the different types of expanders are represented with different isentropic efficiencies. However, in reality, a heat source's heat flux and temperature may vary depending on its type, constant temperatures, and heat fluxes were assumed for simplicity in the outlined cases. While this may be a reasonable assumption for a geothermal well or a three-shift industrial process, it has to be noted that real-world scenarios may be more complex.

As the main goal was to identify suitable working fluids for reaching the low-threshold technology, and the publicly available, high-accuracy database only consists of 69 potential options, no pre-screening was conducted. Therefore, the results presented below may not offer a realistic alternative due to additional constraints that could impede their implementation. Nonetheless, by expanding the database and preselecting the media based on additional criteria, it is possible to significantly narrow down the options for real ideal working fluids.

It should also be noted that expander efficiency is influenced not only by the expander's type, size, and geometry but also by the working fluid and the external conditions (mainly the temperature range). Therefore, a

rough estimate for the internal efficiency might be given based on the expanders' type, size, and geometry, but the exact value has to be determined for every application specifically.[41,42]

7.1 | Case 1—cryogenic source

First, the working fluid selection for an ORC installed on a cryogenic cycle is shown with $T_L = 193\ K = -80°C$ and $T_U = 300 = 27°C$ for maximal (upper) and minimal (lower) expansion temperatures. The lower temperature limit might be reached when utilizing the "cold energy" from an LNG regasification process, where temperatures can be as low as −162°C. However, such low-temperature heat cannot be used directly in an ORC due to the threat of brittle failure. With liquid natural gas as a coolant, reducing the temperature of the working fluid only to a moderate level (e.g., −80°C) and applying the appropriate material (in this case, austenitic stainless steel), the problem can be addressed.[43]

The radial turbine is a commonly used expander for cryogenic sources. Table 1 shows that its isentropic efficiency varies widely depending on the working fluid and power output, therefore, it has been set at 70%. Figure 13A shows part of the T_L–T_U diagram at 70% isentropic efficiency, with the gray star symbolizing the maximal–minimal temperature pair. This operating point is located in the immediate vicinity of the ACZ type R134a (811-97-2), which makes this working fluid favorable for the given conditions. Figure 13B, displaying the T–s diagram of R134a, shows the expansion through the superheated vapor region only before terminating in the saturated vapor state at 193 K (−80°C).

Since selecting the working fluid is a multi-dimensional optimization process, it is appropriate to consider pressure as the following parameter. Although R134a appears to be the best match based on the selection method, the pressure at the endpoint of the expansion (at 193 K) is only 3.63 kPa, which is lower than the 5–10 kPa common in real power plants. Therefore, another working fluid, which was found to be ideal based on the selection procedure, was also investigated. The

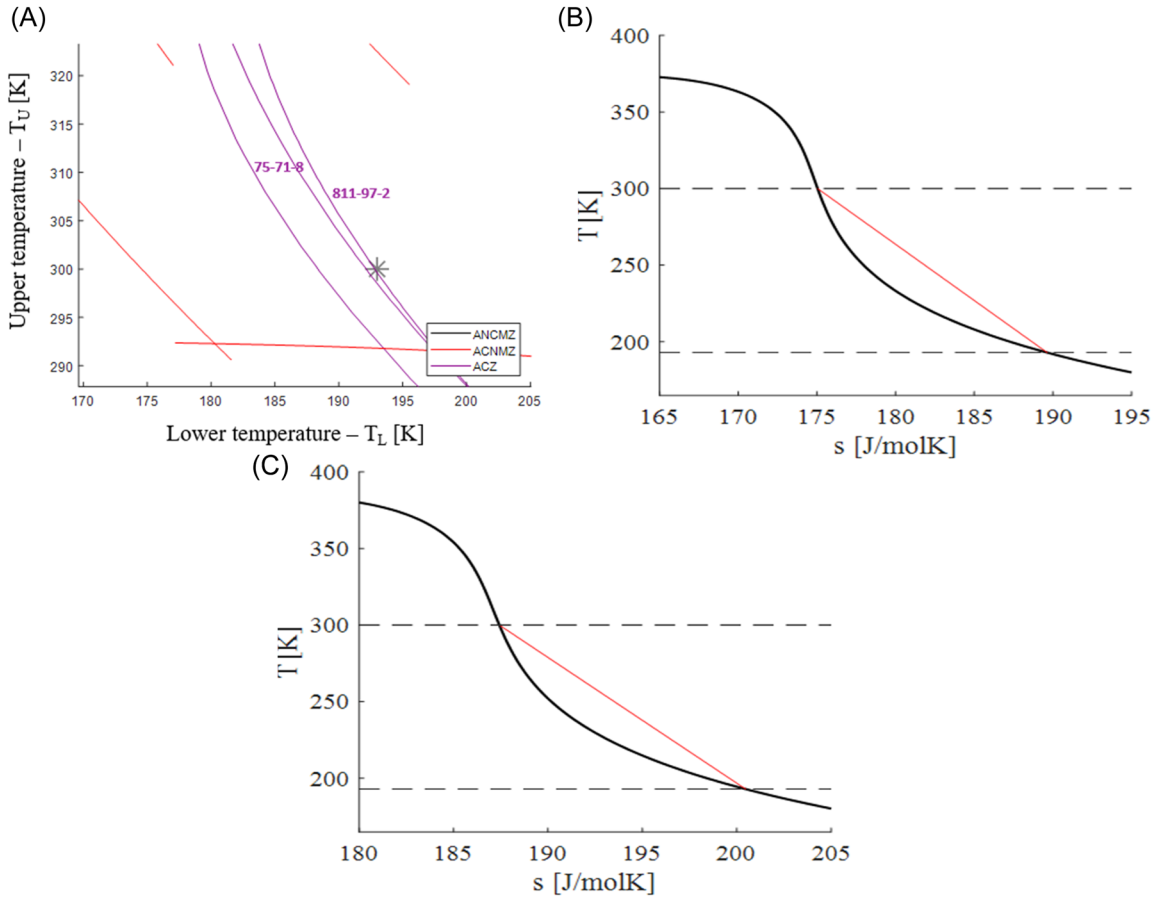

FIGURE 13 (A) Magnified part of the potential expansion routes at 70% isentropic efficiency centered on the 193–300 K point. The expansion process of R134a, CAS 811-97-2 (B) and R12, CAS 75-71-8 (C) on T–s diagram for a given T_L–T_U pair (193–300 K) with 70% isentropic efficiency.

curve representing R12 (CAS 75-71-8) in Figure 13A is also in the vicinity of the operating point and, as can be seen from the *T*–*s* diagram showing the expansion (Figure 13C), the endpoint of the process is so close to the saturation curve that no significant droplet formation is expected. In this case, the pressure at the endpoint is 6.12 kPa, which is more acceptable. Nevertheless, it is crucial to emphasize that while the material is beneficial for achieving a straightforward layout and its low toxicity and flammability make it appealing, it cannot be considered a viable alternative for real-life implementation due to its significantly high GWP and ODP.

7.2 | Case 2–geothermal source

In the second case, a shallow, low-yielding geothermal well is considered with natural water as a heat sink to show results in which a technically superior solution may not offset the expenses associated with the investment. The heat reservoir is assumed to have a temperature range between $T_L = 293\ K = 20°C$ and $T_U = 403\ K = 130°C$. Due to the low expected capacity, a low-efficiency screw expander could be an appropriate choice. Based on Table 1, for this case, 64% efficiency was set. The operating point in Figure 14A with 64% isentropic efficiency is slightly below the line representing the ACZ type dichlorofluoromethane (75-43-4), which means that the presented expansion ends in the wet region. However, the endpoint of the expansion is so close to the saturated vapor state—as shown in Figure 14B—that neither cycle efficiency degradation nor blade erosion is a genuine risk. Similar to the previous solution, while it may possess desirable characteristics, it has also been phased out in the past due to its highly detrimental environmental effects, such as having an extremely high GWP and ODP.

7.3 | Case 3—industrial waste heat source

In the third case, a working fluid is selected for an ORC to recover medium-temperature industrial waste heat, for example, from the ceramic, steel, or glass industry. The operating point—marked with the gray star in Figure 15A—is at $T_L = 290\ K = 17°C$ and $T_U = 456\ K = 183°C$ on the expansion route map.[44] If the technology requires the utilization of several MW_{th} of waste heat, an axial turbine could be a suitable option. While not listed in Table 1, this type of turbine can attain significantly greater efficiency than the alternatives mentioned in the previous case. For this example, an 89% isentropic efficiency was chosen, typical for an axial turbine. For these parameters, the operating point on the T_L–T_U map is slightly above the line representing the favorable working fluid, ACNMZ type trichlorofluoromethane (75-69-4). Regarding the *T*–*s* diagram of the chosen fluid (Figure 15B), it is visible that the expansion initiates from the C–M section of the saturated vapor curve; hence a large part of the expansion is in the two-phase region. However, as mentioned above, blade erosion caused by droplet formation is still not a substantial problem. The endpoint of the expansion is in the superheated dry vapor region but so close to the saturation curve that no significant efficiency loss is expected. The temperature gap between the endpoint and the saturation curve reached by isentropic expansion is approximately 0,05 K,

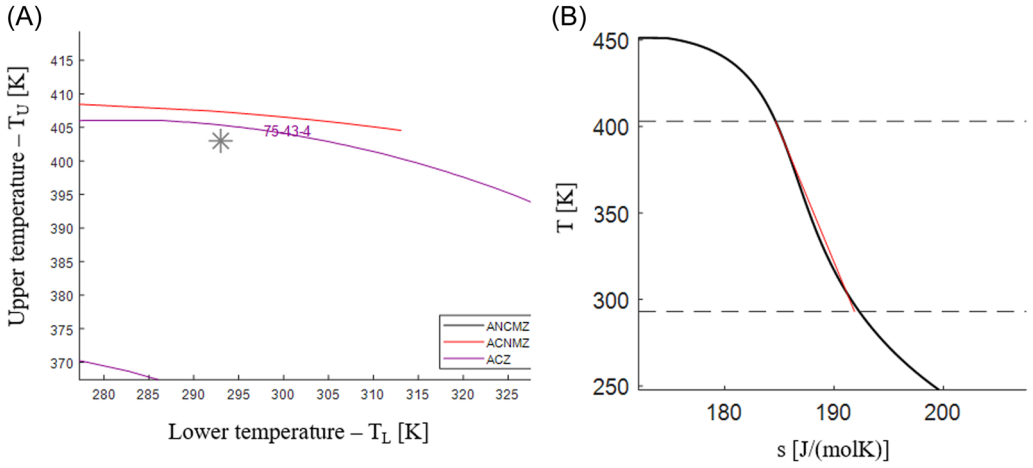

FIGURE 14 (A) Magnified part of the potential expansion routes map at 64% isentropic efficiency centered on the 293–403 K point. (B) Expansion process of dichlorofluoromethane, CAS 75-43-4 on *T*–*s* diagram for a given T_L–T_U = pair (293–403 K) with 64% isentropic efficiency.

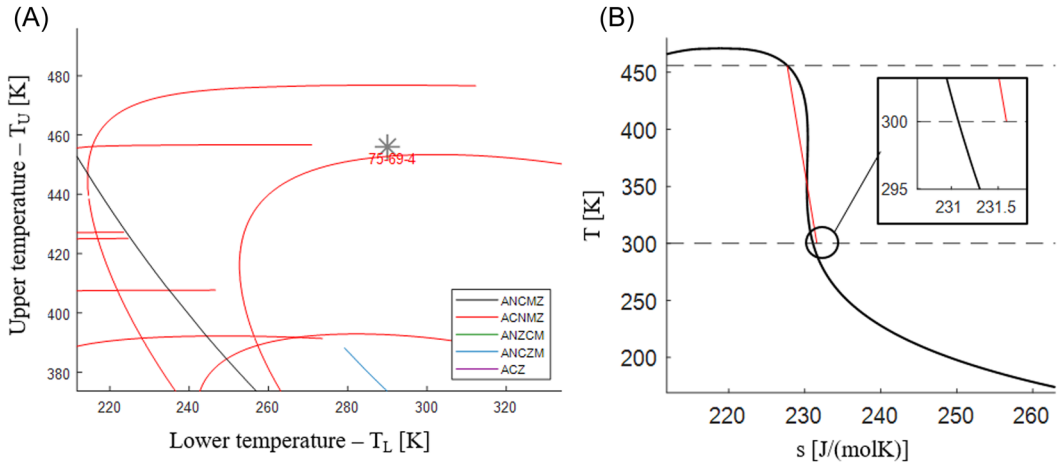

FIGURE 15 (A) Magnified part of the potential expansion routes map at 89% isentropic efficiency centered on the 290–456 K point. (B) The expansion process of trichlorofluoromethane, CAS 75-69-4 on *T*–*s* diagram for a given T_L–T_U = pair (290–456 K) with 89% isentropic efficiency.

which is practically within the measuring error range, and therefore, no recuperative heat recovery is needed.

The substance was formerly employed as a refrigerant in highly specialized cooling systems. However, similar to the other two substances, it was also eliminated because of its high GWP and ODP.

8 | SUMMARY

The ORC can be technically a suitable solution for utilizing small flux heat sources. However, the produced power—and, therefore, the income—can pose strict limits for installation costs. One of the ways to minimize this cost is by using the basic ORC layout—a pump, a heat exchanger (for liquid heating and evaporation), an expander, and a second heat exchanger (for condensation). This way, the installation of extra parts (like superheater, recuperator) can be omitted. Additionally, the amount of residual heat and the wetness of the expanded steam have to be minimized to avoid efficiency losses. Both goals can be achieved if the expansion starts and terminates exactly in (or at least in the very close vicinity of) saturated vapor states. Theoretically, it can be done by using an isentropic working fluid with an ideal expansion process, but none of them—neither an isentropic working fluid nor an ideal expansion process—exist.

This paper described a novel working fluid selection where potential working fluids and real expansion processes (given by the expander internal efficiency values) could be obtained simultaneously by giving an expander input-output temperature pair. The results are based on the previous classification scheme of *T*–*s* diagrams of Györke et al.[21,22]

Software and a database were created for this process; presently, the expandable database contains a pool of 69 potential working fluids taken from the NIST Chemistry Webbook.[38] Some working fluids are from the so-called real isentropic category with inverse S-shaped saturated vapor lines, while others are classified as wet fluids. Real isentropes—usually with higher expander efficiencies, above 70%—are given as matches for low-temperature ORC-s; for higher temperature ones, wet working fluids with low expander efficiencies—usually below 80%—offer a better solution. The expander type is also indicated in obtaining a working fluid-expansion efficiency pair for a given type of heat source.

The use of the selection method was demonstrated in three cases by finding the best matching working fluid for a small ORC system fitted to an (i) industrial waste heat, (ii) a low-temperature geothermal, and (iii) a cryogenic heat source. It can be seen from these demonstrations that the proposed method (together with the freely available software) can be a good tool for ORC working fluid selection processes when installation and maintenance costs should be lowered and efficiency and gross power losses caused by wetness (during expansion) or residual heat (after the expansion) will be minimized or completely eliminated.

Based on the previous paragraphs, the results can be summarized in the following points:

(1) The importance of using "saturated vapor to saturated vapor" expansion routes for the design of small-power ORC systems was discussed.

(2) The theoretical background to select "saturated vapor to saturated vapor" expansion routes for real (non-isentropic) processes was presented.
(3) A simultaneous working fluid and expander selection method was developed to simplify the layout.
(4) Software using this method and using maximal and minimal expansion temperatures as input and giving fitting working fluids paired with expansion devices (characterized by their internal efficiency) was developed.
(5) Three cases (using cryogenic, geothermal, and waste heat sources) were shown to demonstrate the method.

Since the working fluid selection is a multi-dimensional optimization process, other criteria (economic, environmental, etc.) obviously must be considered, and the final decision must be based on a complex optimization process. Nevertheless, as the objective of the process is to reduce the system's complexity, which may lead to a low-entry threshold technology, the low-efficiency expanders suggested by the selection algorithm may also introduce previously overlooked media categories.

ACKNOWLEDGMENTS

The research was funded by the Sustainable Development and Technologies National Program of the Hungarian Academy of Sciences (FFT NP FTA). Part of the research reported in this paper and carried out at BME has been supported by the NRDI Fund (TKP2020 NC, Grant No. BME-NC) based on the charter of bolster issued by the NRDI Office under the auspices of the Ministry for Innovation and Technology. One of the authors was also supported by the ÚNKP-21-5 New National Excellence Program of the Ministry for Innovation and Technology from the source of the National Research, Development and Innovation Fund and by the János Bolyai Research Scholarship of the Hungarian Academy of Sciences.

ORCID

Axel Groniewsky http://orcid.org/0000-0002-7966-4218

REFERENCES

1. Shi X, Wang X, Cai J, Gao Y, Tian H, Shu G. A novel design method of organic Rankine cycle system harvesting waste heat of heavy-duty trucks based on off-design performance. *Energy Sci Eng*. 2021;9(2):172-188. doi:10.1002/ese3.838
2. Papadopoulos AI, Stijepovic M, Linke P. On the systematic design and selection of optimal working fluids for organic rankine cycles. *Appl Therm Eng*. 2010;30(6–7):760-769. doi:10.1016/j.applthermaleng.2009.12.006
3. Bobbo S, Nicola GD, Zilio C, Brown JS, Fedele L. Low GWP halocarbon refrigerants: a review of thermophysical properties. *Int J Refrig*. 2018;90:181-201. doi:10.1016/j.ijrefrig.2018.03.027
4. Kondo S, Urano Y, Tokuhashi K, Takahashi A, Tanaka K. Prediction of flammability of gases by using F-number analysis. *J Hazard Mater*. 2001;82(2):113-128. doi:10.1016/S0304-3894(00)00358-7
5. Reid RC, Prausnitz JM, Poling BE. *The Properties of Gases and Liquids*. McGraw Hill Book Co.; 1987.
6. Buxton A, Livingston AG, Pistikopoulos EN. Optimal design of solvent blends for environmental impact minimization. *AIChE J*. 1999;45(4):817-843. doi:10.1002/aic.690450415
7. Sastri SRS, Rao KK. A new method for predicting saturated liquid viscosity at temperatures above the normal boiling point. *Fluid Phase Equilib*. 2000;175(1–2):311-323. doi:10.1016/S0378-3812(00)00472-6
8. Sastri SRS, Rao KK. A new temperature-thermal conductivity relationship for predicting saturated liquid thermal conductivity. *Chem Eng J*. 1999;74(3):161-169. doi:10.1016/S1385-8947(99)00046-7
9. Constantinou L, Gani R. New group contribution method for estimating properties of pure compounds. *AIChE J*. 1994;40(10):1697-1710. doi:10.1002/aic.690401011
10. Calm JM, Didion DA. Trade-offs in refrigerant selections: past, present, and future compromis dans le choix de frigorig nes: pass6, pr6sent et futur. *Int J Refrig*. 1998;21(4):308-321. [Online]. doi:10.1080/23744731.2015.1009353
11. Bahrami M, Pourfayaz F, Kasaeian A. Low global warming potential (GWP) working fluids (WFs) for organic Rankine cycle (ORC) applications. *Energy Reports*. 2022;8:2976-2988. doi:10.1016/j.egyr.2022.01.222
12. Wang Y, Qin G, Zhang Y, et al. Conventional and advanced exergy analyses of an organic Rankine cycle by using the thermodynamic cycle approach. *Energy Sci Eng*. 2021;9(12):2474-2492. doi:10.1002/ese3.980
13. Wang Q, Macián-Juan R, Li D. Analysis and assessment of a novel organic flash Rankine cycle (OFRC) system for low-temperature heat recovery. *Energy Sci Eng*. 2022;10(8):3023-3043. doi:10.1002/ese3.1186
14. Mohammadi A, Ashouri M, Ahmadi MH, Bidi M, Sadeghzadeh M, Ming T. Thermoeconomic analysis and multiobjective optimization of a combined gas turbine, steam, and organic Rankine cycle. *Energy Sci Eng*. 2018;6(5):506-522. doi:10.1002/ese3.227
15. González J, Llovell F, Gonz alez J, Quinteros-Lama H. A rigorous approach for characterising the limiting optimal efficiency of working fluids in organic Rankine cycles. *Energy*. 2022;254:124191. doi:10.1016/j.energy.2022.124191
16. Morrison G. The shape of the temperature-entropy saturation boundary. *Int J Refrig*. 1994;17(7):494-504.
17. Kolasiński P. Application of volumetric expanders in small vapour power plants used in distributed energy generation—selected design and thermodynamic issues. *Energy Convers Manage*. 2021;231:113859. doi:10.1016/j.enconman.2021.113859
18. Zhang X, Zhang Y, Wang J. Evaluation and selection of dry and isentropic working fluids based on their pump performance in small-scale organic Rankine cycle. *Appl Therm Eng*. 2021;191:116919. doi:10.1016/j.applthermaleng.2021.116919

19. Garrido JM, Quinteros-lama H, Mejía A, Wisniak J, Segura H. A rigorous approach for predicting the slope and curvature of the temperature–entropy saturation boundary of pure fluids. *Energy*. 2012;45(1):888-899. doi:10.1016/j.energy.2012.06.073
20. Tabor H, Bronicki L. *Establishing criteria for fluids for small vapor turbines*; 1964. doi:10.4271/640823
21. Györke G, Deiters UK, Groniewsky A, Lassu I, Imre AR. Novel classification of pure working fluids for organic Rankine cycle. *Energy*. 2018;145:288-300. doi:10.1016/j.energy.2017.12.135
22. Imre AR, Kustán R, Groniewsky A. Thermodynamic selection of the optimal working fluid for organic Rankine cycles. *Energies*. 2019;12(10):2028. doi:10.3390/en12102028
23. Linstrom P. *NIST Chemistry WebBook*. NIST; *Standard Reference Database Number 69*; 1997.
24. NIST. RefProp 9.1. 2021. [Online]. https://www.nist.gov/srd/refprop
25. White JA, Velasco S. Characterizing wet and dry fluids in temperature-entropy diagrams. *Energy*. 2018;154:269-276. doi:10.1016/j.energy.2018.04.105
26. Kustán R, Imre AR, Groniewsky A, "The effect of internal efficiency of expander on the working fluid selection. IIR International Rankine 2020 Conference—Heating, Cooling and Power Generation—Refrigeration Science and Technology, 2020:351-357, doi:10.18462/iir.rankine.2020.1170.
27. Imre AR, Kustán R, Groniewsky A. Thermodynamic selection of the optimal working fluid. Proceedings of the 5th International Seminar on ORC Power Systems, 2019:156.
28. Baldasso E, Mondejar ME, Mazzoni S, Romagnoli A, Haglind F. Potential of liquefied natural gas cold energy recovery on board ships. *J Clean Prod*. 2020;271:122519. doi:10.1016/j.jclepro.2020.122519
29. Choi HW, Na S-I, Hong SB, Chung Y, Kim DK, Kim MS. Optimal design of organic Rankine cycle recovering LNG cold energy with finite heat exchanger size. *Energy*. 2021;217:119268. doi:10.1016/j.energy.2020.119268
30. Xu B, Rathod D, Yebi A, Filipi Z, Onori S, Hoffman M. A comprehensive review of organic rankine cycle waste heat recovery systems in heavy-duty diesel engine applications. *Renew Sustain Energy Rev*. 2019;107:145-170. doi:10.1016/j.rser.2019.03.012
31. Yue C, Wang P. Thermal analysis on vehicle energy supplying system based on waste heat recovery ORC. *Energy Proc*. 2019;158:5587-5595. doi:10.1016/j.egypro.2019.01.582
32. Hughes FR, Starzmann J, White AJ. Nucleation and wake-chopping in low pressure steam turbines. *Proc Inst Mech Eng Part A J Power Energy*. 2018;232(5):490-500. doi:10.1177/0957650917736454
33. Nezbeda I, Moučka F. Thermodynamics of supersaturated steam: towards an equation of state. *Fluid Phase Equilib*. 2019;484:114-121. doi:10.1016/j.fluid.2018.11.028
34. Leĭzerovich AS. Wet-steam Turbines for Nuclear Power Plants. PennWell Corporation, 2005.
35. White MT. Investigating the wet-to-dry expansion of organic fluids for power generation. *Int J Heat Mass Transfer*. 2022;192:122921. doi:10.1016/j.ijheatmasstransfer.2022.122921
36. Imre A, Kustán R, Groniewsky A. Mapping of the temperature–Entropy diagrams of van der Waals Fluids. *Energies*. 2020;13(6):1519. doi:10.3390/en13061519
37. Imre AR, Groniewsky A, Györke G, Katona A, Velmovszki D. Anomalous properties of some fluids—with high relevance in energy engineering—in their pseudo-critical (Widom) region. *Period Polytech Chem Eng*. 2019;63(2):276-285. doi:10.3311/PPch.12905
38. Lemmon EW, McLinden MO, Friend DG. NIST Chemistry WebBook, NIST Standard Reference Database. 2017;69.
39. Zhao Y, Liu G, Li L, Yang Q, Tang B, Liu Y. Expansion devices for organic rankine cycle (ORC) using in low temperature heat recovery: a review. *Energy Convers Manage*. 2019;199:111944. doi:10.1016/j.enconman.2019.111944
40. Shahrooz M, Lundqvist P, Nekså P. Effect of working fluid type on low temperature Rankine (no. September); 2019:1-8. https://www.researchgate.net/publication/335857810_Effect_of_Working_Fluid_Type_on_Low_Temperature_Rankine_Cycle_Optimization
41. Capata R, Pantano F. Expander design procedures and selection criterion for small rated organic rankine cycle systems. *Energy Sci Eng*. 2020;8(10):3380-3414. doi:10.1002/ese3.710
42. Jia W, Wang C, Zhang K, Feng S, Yan J, Liu B. Analysis of impeller blade parameters and tip clearance of turboexpander in organic Rankine cycle system. *Energy Sci Eng*. 2019;7(6):3283-3296. doi:10.1002/ese3.498
43. Fultz BS. *The Challenges of LNG Materials Selection*; 2014. https://www.bechtel.com/.
44. Peris B, Navarro-Esbrí J, Molés F, Mota-Babiloni A. Experimental study of an ORC (organic Rankine cycle) for low grade waste heat recovery in a ceramic industry. *Energy*. 2015;85:534-542. doi:10.1016/j.energy.2015.03.065

SUPPORTING INFORMATION

Additional supporting information can be found online in the Supporting Information section at the end of this article.

How to cite this article: Groniewsky A, Kustán R, Imre AR. Simultaneous working fluid and expander selection method for reaching low-threshold technology organic Rankine cycle (ORC) design. *Energy Sci Eng*. 2023;11:2330-2350. doi:10.1002/ese3.1457

APPENDIX A

Currently, available working fluids with their common name, CAS number and R-number (if available) are shortlisted in Table A.1.

TABLE A.1 List of working fluids available for selection in ORC-WFS program.

Name	Formula	CAS Registry Number	Refrigerant number
methane	CH4	74-82-8	R50
ethane	C2H6	74-84-0	R170
propane	C3H8	74-98-6	R290
butane	C4H10	106-97-8	R600
2-methylpropane (isobutane)	C4H10	75-28-5	R600a
pentane	C5H12	109-66-0	R601
2-methylbutane (isopentane)	C5H12	78-78-4	R601a
hexane	C6H14	110-54-3	
2-methylpentane (isohexane)	C6H14	107-83-5	
heptane	C7H16	142-82-5	
octane	C8H18	111-65-9	
nonane	C9H20	111-84-2	
decane	C10H22	124-18-5	
trichlorofluoromethane	CCl3F	75-69-4	R11
dichlorodifluoromethane	CCl2F2	75-71-8	R12
chlorotrifluoromethane	CClF3	75-72-9	R13
tetrafluoromethane	CF4	75-73-0	R14
dichlorofluoromethane	CHCl2F	75-43-4	R21
chlorodifluoromethane	CHClF2	75-45-6	R22
trifluoromethane	CHF3	75-46-7	R23
difluoromethane	CH2F2	75-10-5	R32
fluoromethane	CH3F	593-53-3	R41
freon 113	C2Cl3F3	76-13-1	R113
freon 115	C2ClF5	76-15-3	R115
freon 116	C2F6	76-16-4	R116
freon 123	C2HCl2F3	306-83-2	R123
freon 124	C2HClF4	2837-89-0	R124
pentafluoroethane	C2HF5	354-33-6	R125
ethane, 1,1,1,2-tetrafluoro-	C2H2F4	811-97-2	R134a
1,1-dichloro-1-fluoroethane	C2H3Cl2F	1717-00-6	R141b
ethane, 1-chloro-1,1-difluoro-	C2H3ClF2	75-68-3	R142b
ethane, 1,1,1-trifluoro-	C2H3F3	420-46-2	R143a
1,1-difluoroethane	C2H4F2	75-37-6	R152a

TABLE A.1 (Continued)

Name	Formula	CAS Registry Number	Refrigerant number
perfluoropropane	C3F8	76-19-7	R218
propane, 1,1,1,2,3,3,3-heptafluoro-	C3HF7	431-89-0	R227ea
1,1,1,2,3,3-hexafluoropropane	C3H2F6	431-63-0	R236ea
1,1,1,3,3,3-hexafluoropropane	C3H2F6	690-39-1	R236fa
1,1,2,2,3-pentafluoropropane	C3H3F5	679-86-7	R245ca
1,1,1,3,3-pentafluoropropane	C3H3F5	460-73-1	R245fa
benzene	C6H6	71-43-2	
toluene	C7H8	108-88-3	
decafluorobutane	C4F10	355-25-9	
sulfur dioxide	O2S	7446-09-5	
hydrogen sulfide	H2S	7783-06-4	
sulfur hexafluoride	F6S	2551-62-4	
carbonyl sulfide	COS	463-58-1	
carbon dioxide	CO2	124-38-9	R744
water	H2O	7732-18-5	R718
ammonia	H3N	7664-41-7	R717
nitrogen	N2	7727-37-9	
hydrogen	H2	1333-74-0	
deuterium	D2	7782-39-0	
oxygen	O2	7782-44-7	
fluorine	F2	7782-41-4	
carbon monoxide	CO	630-08-0	
nitrous oxide	N2O	10024-97-2	
deuterium oxide	D2O	7789-20-0	
methanol	CH4O	67-56-1	
ethylene	C2H4	74-85-1	
propene	C3H6	115-07-1	
propyne	C3H4	74-99-7	
cyclopropane	C3H6	75-19-4	
cyclohexane	C6H12	110-82-7	
helium	He	7440-59-7	
neon	Ne	7440-01-9	
argon	Ar	7440-37-1	
krypton	Kr	7439-90-9	
xenon	Xe	7440-63-3	
nitrogen trifluoride	F3N	7783-54-2	

APPENDIX B

The purpose of the Working Fluid Selector (ORC-WFS v1.3) is to select the optimal working fluid for a given heat source and sink pair; characterized by the corresponding estimated maximal and minimal expansion temperatures.

With this software, a working fluid can be selected from an experimental database, with which a real expansion process between a given upper (T_U) and lower temperature (T_L) is feasible in such a way that the initial and final states are both in saturated vapor states.

DATA base—Fluids: This software version uses 69 pure working fluids with T-s data taken from NIST Chemistry Webbook (2018) and RefProp 9.1 (2013). The categorization of the working fluids was based on the new classification system. A different color was assigned to each group depending on the position of the fluids' primary and secondary characteristic points on the *T*–*s* saturation curve. The fluids are marked by their CAS numbers.

Color coding: ANCMZ—black, ACNMZ—red, ANZCM—green, ANCZM—blue, ACZ—purple.

Working fluid selection: The selection process uses the temperature pair defined by the User. This creates a mark (gray star) on the expansion route map. The fluids approaching the predefined T_L–T_U point with the given accuracy (± 5 K) go to the "optimal fluid pool." The hits are displayed in a spreadsheet under their corresponding internal efficiency with their CAS number. The selection process is realized between 100% and 50% expander internal efficiency with 1% increments. Once the selection process is complete, a video of the potential expansion routes of different working fluids that initiate and terminate in a saturated vapor state will be available (Figure A1).

The working fluid selector can be obtained from the authors (for reasonable request) and can be used freely for educational and research purposes. A short video showing the use of the program is attached as a supplementary file (link will be inserted later).

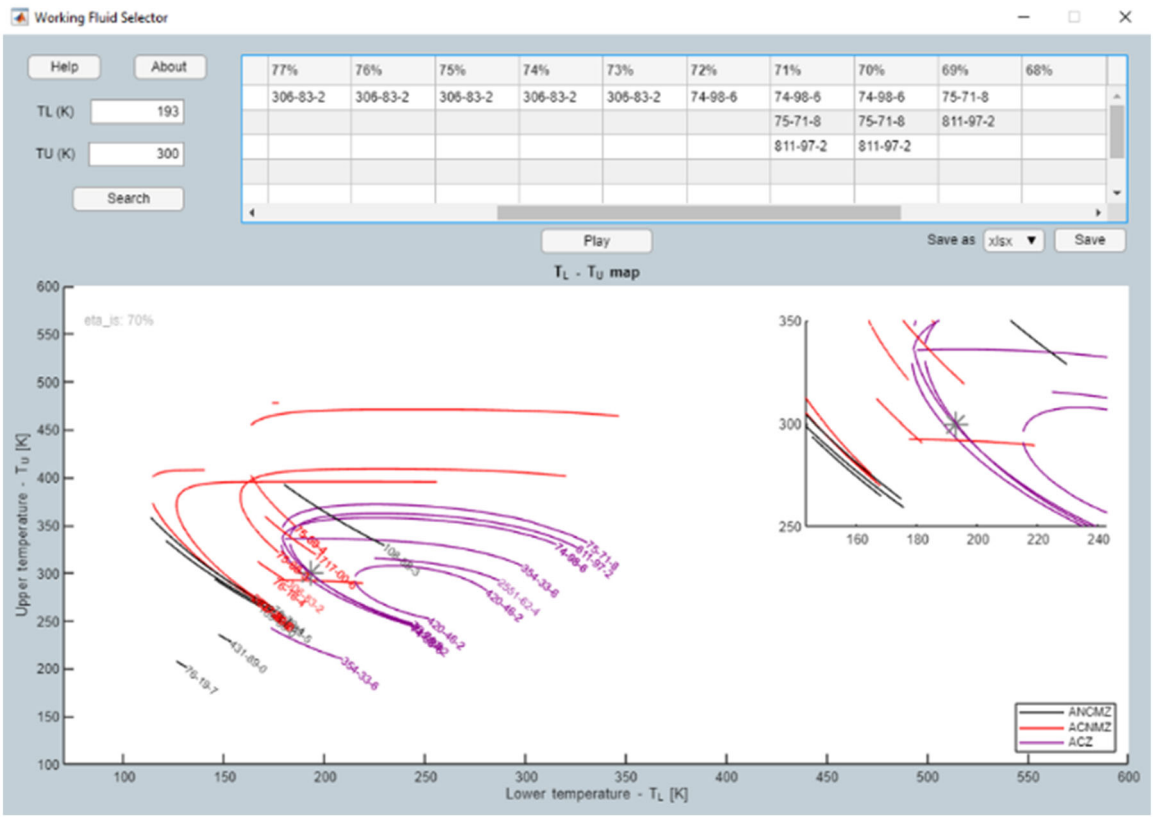

FIGURE A1 Screenshot of the ORC-WFS program for Case 1—cryogenic source.